Semiconductor Physics, Quantum Electronics & Optoelectronics, 2013. V. 16, N 4. P. 331-335.

PACS 61.66.Dk, -f; 61.72.Cc, J-, Tt; 61.82.Fk; 71.55.Cn

Tin doping effect on crystallization of amorphous silicon obtained by vapor deposition in vacuum

V.B. Neimash[1], V.M. Poroshin[1], P.Ye. Shepeliavyi[2], V.O. Yukhymchuk[2], V.V. Melnyk[3], V.A. Makara[3], A.G. Kuzmich[3]
[1]*Institute of Physics, NAS of Ukraine, 46, prospect Nauky, 03028 Kyiv, Ukraine*
[2]*V. Lashkaryov Institute of Semiconductor Physics, NAS of Ukraine, 45, prospect Nauky, 03028 Kyiv, Ukraine*
[3]*Taras Shevchenko Kyiv National University, Physics Department, 60, Volodymyrska str., 01601 Kyiv, Ukraine*

Abstract. The influence of tin impurity on amorphous silicon crystallization was investigated using the methods of Raman scattering, Auger spectroscopy at ion etching, scanning electron microscopy and X-ray fluorescence microanalysis in thin films of Si:Sn alloy manufactured by thermal evaporation. Formation of Si crystals of the 2 to 4-nm size has been found in the amorphous matrix alloy formed at the temperature 300 °C. Total volume of nanocrystals correlates with the content of tin and can comprise as much as 80% of the film. The effect of tin-induced crystallization of amorphous silicon occurred only if there are clusters of metallic tin in the amorphous matrix. The mechanism of tin-induced crystallization of silicon that has been proposed takes into account the processes in eutectic layer at the interface metal tin – amorphous silicon.

Keywords: nanocrystalline silicon, amorphous silicon, thin films, Si:Sn alloy.

Manuscript received 06.08.13; revised version received 26.09.13; accepted for publication 23.10.13; published online 16.12.13.

1. Introduction

Nanocrystalline silicon thin films are one of the most promising materials for photovoltaic solar energy cells [1-3]. Controlled crystallization of amorphous silicon films could be one of the ways to produce nanocrystalline silicon. It is known very little about the effect of tin doping on the transformation of silicon from amorphous to crystalline state. Tin as an element of group IV is isovalent impurity in silicon. Since Sn does not create energy levels in Si band gap (E_g), tin doping does not affect electrical, optical and recombination properties of Si crystals. At the same time, Sn atoms available in Si significantly slow down the degradation of these characteristics caused by heating [4-6] and radiation [6-8]. The first reports about crystallization of $a-\mathrm{Si}$ films doped by Sn from the gaseous phase in the process of film formation were made in [9]. Their results were further confirmed in [10], where the dominant size of Si crystals in amorphous matrix was close to few nanometers. However, the distribution of Sn atoms inside the film of Si:Sn alloy produced by the authors of [9] was very heterogeneous. Therefore, the aim of this work was to study of the effect of different Sn concentrations on phase state Si:Sn alloy with controlled distribution of Sn in the layers suitable for Raman scattering method investigation.

2. Experiment

Si:Sn alloy films with the thickness from the range 300 to 500 nm were prepared from high-purity powder mixtures of Si and Sn taken in different weight ratios by thermal sputtering in vacuum. The films were deposited on silica or monocrystalline Si substrates at the temperature 300 °C and residual pressure 10^{-3}Pa. The

© 2013, V. Lashkaryov Institute of Semiconductor Physics, National Academy of Sciences of Ukraine

parameters of sputtering ensured a uniform distribution of Sn impurity in 100 nm thick surface layer of the film [10]. Phase composition of the films was determined by analyzing the spectra of Raman scattering (RS) activated by Ar-Kr^{+}-laser at the wavelength 514.5 nm. The impurity distribution profile in the alloy film thickness was investigated by the Auger spectroscopy method at layered ion etching. The surface relief and impurity distribution were investigated by scanning electron microscopy (SEM) and X-ray fluorescence microprobe.

3. Results and discussion

Fig. 1 shows typical profiles of impurity concentrations in Si:Sn alloy films (a) and reference sample of amorphous silicon without tin (b) produced by the known method on the substrate of monocrystalline silicon with SiO_2 layer. It is seen that the films contain technological impurities carbon and oxygen. The concentration distribution of impurities in the surface layer suitable for RS light excitation is shown in Fig. 2.

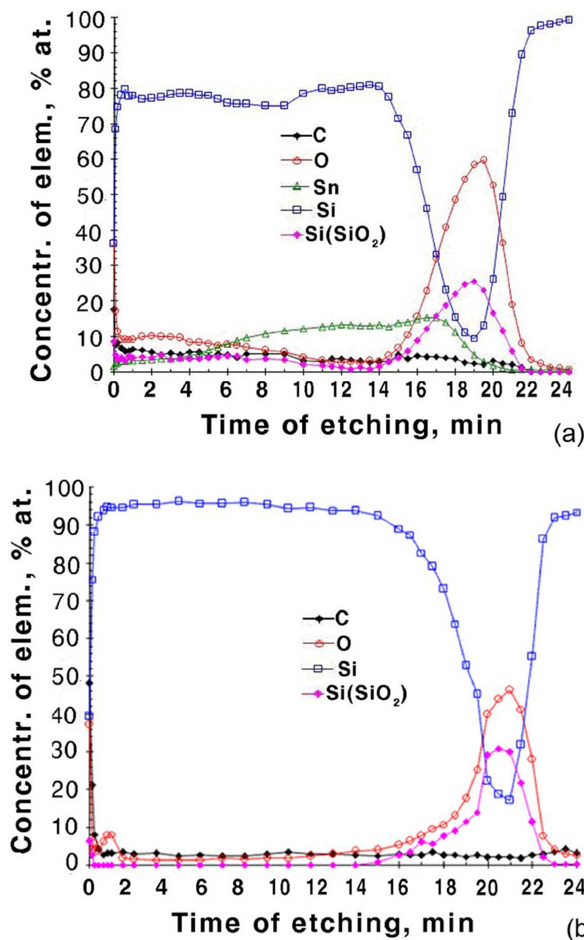

Fig. 1. Distribution profiles of elements: (a) in Si:Sn alloy (Sn concentration 5 at.%); (b) in the reference film of amorphous Si (without Sn).

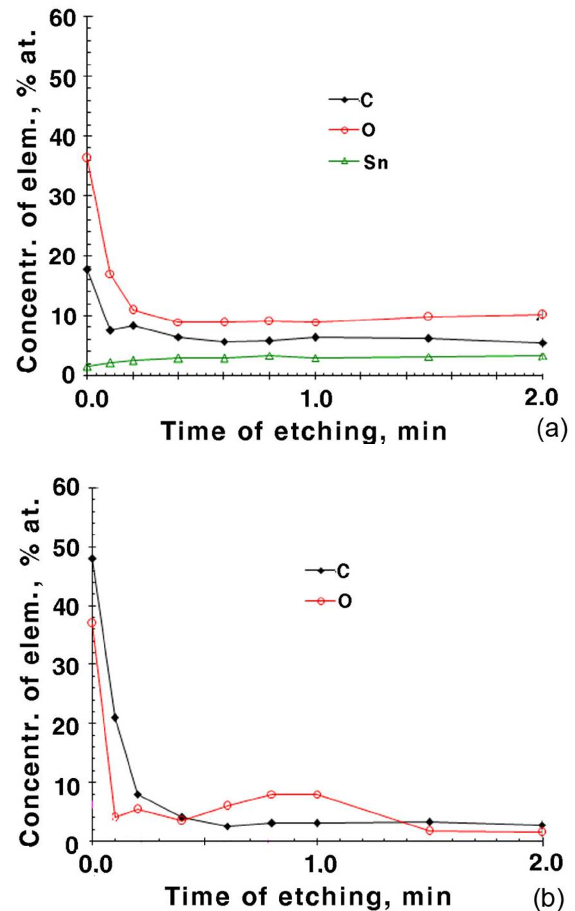

Fig. 2. Distribution profiles of the elements in the surface layer of films doped by tin (a) and in the reference one (b).

As seen in the figure, the distribution of Sn is uniform. The distribution of technological impurities (O and C) is approximately the same in both materials. Qualitatively similar profiles are observed in the films with different tin content. This allows the correct use of RS to analyze the phase structure of alloys. Fig. 3a shows the changes in Raman spectra with increase in the tin content. The wide band at 470 cm^{-1} corresponds to the amorphous Si. The narrow band at 515 cm^{-1} corresponds to crystalline Si. The amplitude of the latter depends on the fraction of crystalline phase in the whole bulk of material, while the peak frequency position – on the dominating crystallite size [11-13]. It is seen that the band at 515 cm^{-1} is observed only at the Sn concentrations close to 2.5 at.% and higher.

With increasing Sn concentration, the amplitude of this band significantly grows, and it becomes slightly shifted upwards by the frequency. That is, tin stimulates crystallization of silicon by increasing the number of crystals, however, producing little effect on their dominant size. To estimate the volume fraction of crystalline phase, we used the formula taken from [11]:

$$X_c = (I_c/I_a)/(Y(L) + I_c/I_a), \quad (1)$$

© 2013, V. Lashkaryov Institute of Semiconductor Physics, National Academy of Sciences of Ukraine

where I_c, I_a are integrated scattering intensities of crystalline and amorphous components, $Y(L) = 0.1 + \exp(-L/25)$ is the ratio of scattering cross sections of crystalline and amorphous silicon, L is the average crystal size (in nanometers) that can be estimated using the formula [12, 13]:

$$I(\nu) = \int \exp\left[-(qL)^2/(4\pi)^2\right] \Big/ \left[(\nu - \nu(q))^2 + (\Gamma_0/2)^2\right] d^3q\,, \quad (2)$$

where Γ_0 is the half-width of the Si phonon band typical for the single crystal, and $\nu(q)$ are dispersion relations for TO (LO) vibrations. The reliable spectrum in the range 400 to 540 cm^{-1} as a Gauss component characteristic of amorphous silicon as well as asymmetric component described by (2) and corresponding to the nanocrystalline phase allowed us to estimate the proportion between them. For example, Fig. 3b shows this decomposition into components for the alloy containing 2.5 at.% of Sn. Summarized in Table 1 are the results of these calculations for the Sn contents: 2.5, 5.0, 7.5 at.%.

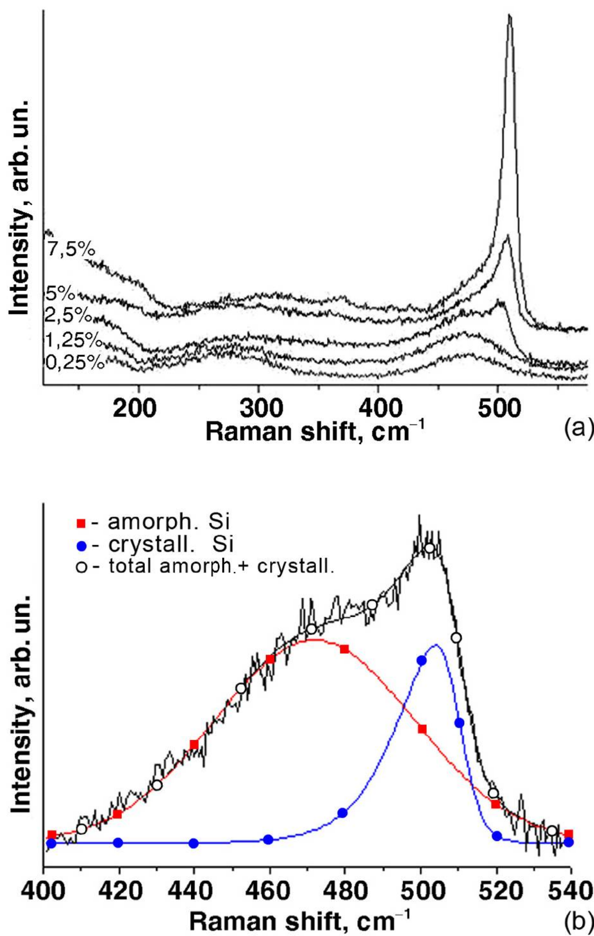

Fig. 3. Raman spectra of Si:Sn alloys with the integral Sn content 0.25…7.5 at.% (a). Decomposition of the Raman spectra into Gaussian components for the amorphous sample doped with 2.5 at.% of Sn (b).

Table 1. The estimated crystal sizes and crystalline phase volumes for the samples containing Sn: 2.5 – 7.5 at.%.

№	Sn, at.%	I_c	I_a	I_c/I_a	Crystal size L (nm)	Crystalline phase X_c (%)
1.	2.5	25.7	75.7	0.34	2.3	0.25
2.	5	45.6	54.4	0.84	2.7	0.46
3.	7.5	61.0	39.1	1.56	3.0	0.61

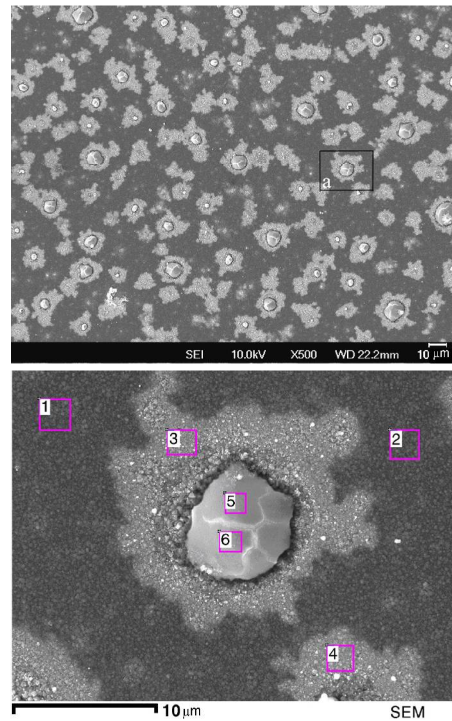

Fig. 4. SEM images of the surface of a silicon film containing 5 at.% of tin. The general view of the surface (on the left). The detailed image of a quasi-spherical formation and dendrite-like aureole (on the right).

In contrast to the reference films (without Sn) and films containing 0.25 and 1.25 at.% of tin, there are quasi-spherical formations surrounded by dendrite-like aureoles on the surface of films listed in Table 1. The size and concentration of these formations correlate with the total Sn concentration. For example, Fig. 4 shows SEM images of the film surface for alloy containing 5 at.% of Sn. The numbered areas in the figure are the action areas of the X-ray microprobe. It is seen that the quasi-spherical formation in the center is a drop of metallic tin. The drop is covered with a typically cracked oxide film. The tin content in halos is twice as high as that outside. To determine the phase state of the film in the region surrounding tin droplets, RS were measured using excitation with the laser microprobe having the diameter close to 1 µm. Fig. 5a shows a photographed image of the surface of the same alloy as in Fig. 4 obtained using an optical microscope. The locations of Raman spectra measured at different distances from the surface of the tin drop are marked by figures.

© 2013, V. Lashkaryov Institute of Semiconductor Physics, National Academy of Sciences of Ukraine

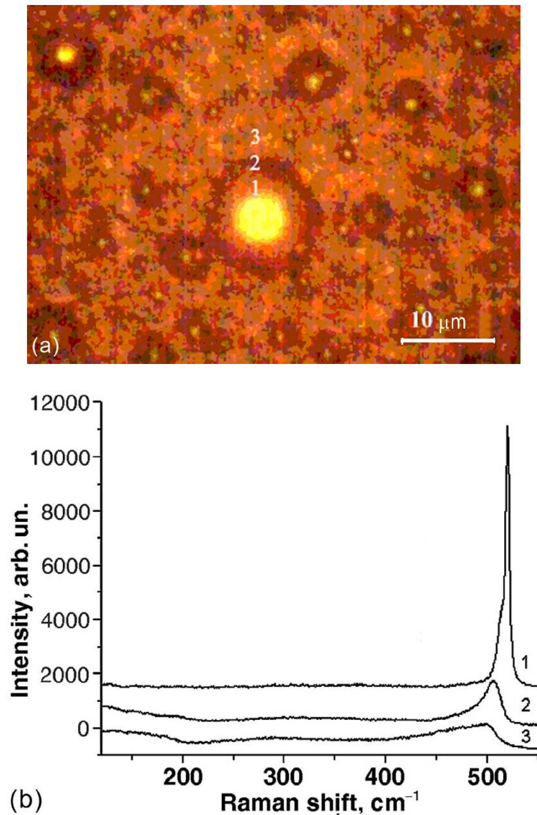

Fig. 5. Designated RS positions of measurements (a) and the respective spectra (b).

Table 2. The results (in atomic %) of the element composition analysis in the areas selected in Fig. 4.

Area №	C	O	Si	Sn
1	3.57	15.59	76.79	4.06
2	3.99	14.75	77.00	4.25
3	3.21	10.80	78.24	7.74
4	3.35	9.56	78.77	8.32
5	4.95	51.45	8.96	34.65
6	5.58	49.62	7.54	37.27

Table 3. The estimated crystal sizes and fraction of the crystalline phase in the film per unit of volume for the regions selected in Fig. 5a.

№	I_c	I_a	I_c/I_a	Crystal size L (nm)	Crystalline phase X_c (%)
1	23.7	5.8	4.09	4.5	80
2	59.8	40.21	1.49	2.7	60
3	28.8	71.2	0.40	2.3	28

Fig. 5b shows RS spectra measured in the locations indicated in Fig. 5a. It is seen that amplitude of the band related with the crystalline phase, estimated within the range 500 to 525 cm^{-1}, increases nearer to the tin drop. The quantitative estimates of silicon crystalline phase in the vicinity of tin droplet obtained by the method of decomposition into amorphous and crystalline components of RS described above when analyzing the spectra in Fig. 3 are shown in Table 3.

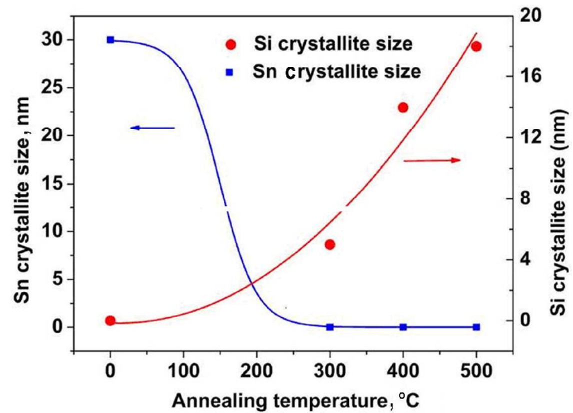

Fig. 6. Dependence of Si and Sn crystal sizes on the annealing temperature [15].

The table shows that the relative fraction of the bulk occupied by Si crystals is 80% near the surface and decreases to 28% at the periphery of the halo. Typically, the crystal size in the middle and the peripheral parts of the halo (i.e., in its main part) is about 2-3 nm, like to the case of integral Raman measurements (Table 1) with the excitation beam diameter close to 30 μm.

It should be noted that no tin droplets are observed on the surface of alloys containing 0.25 and 1.25 at.% of tin (amorphous according to RS). This indicates that silicon crystallizes only in the films containing drops of metallic tin. Crystallization spreads from the interface of metal – amorphous Si into the film bulk. This result agrees with the data from [14] where it was shown that in planar film structure "amorphous Si on crystalline Sn" Si crystallizes and Sn dissolves at the edge of these films in the course of annealing at 300…500 °C. The production of polycrystalline silicon film on metallic substrates by forming a joint eutectic layer due exchange of neighboring atoms of the metal and $a-Si$ films was analyzed in [15] and the "mechanism of exchange layer" was suggested for interpretation.

But direct application of this mechanism to interpret our results does not allow us to explain the dendritic character of crystallization around tin droplets and gradient crystalline phase proximity to a surface tin droplet. Therefore, we propose a slightly different mechanism. We shall consider the Si:Sn eutectic as a solution of silicon in tin which is liquid at 300 °C. $a-Si$ surface dissolves in eutectic until the solution is saturated. Further on the solution can disintegrate with Si crystals formed in it. The crystals' maximum size depends on the solution temperature. Fig. 6 shows the dependence of the grain size on the Si annealing temperature obtained in [15].

The solubility of tin in crystalline silicon is weak (~10^{19} cm^{-3} [16]). Therefore, segregation occurs on the surface of growing Si crystals. Sn atoms return to the eutectic. The solution again becomes unsaturated, and the solution of amorphous silicon is restored. Then the

© 2013, V. Lashkaryov Institute of Semiconductor Physics, National Academy of Sciences of Ukraine

process repeats. Sn segregation on Si crystallization front forms a suitable layer of concentration supercooling of the solution whose fluctuations of thickness cause the characteristic dendritic shape of the crystallization zone. As it can be assumed from Fig. 6, crystal sizes obtained in our experiments (2.3 to 4.5 nm) fall into the region 200…300 °C. This coincides with real cooling our film alloys on substrates heated to 300 °C.

To better understand the mechanism of Sn influence on $a-Si$ crystallization, additional investigations of annealing effect on the Si: Sn alloy microstructure are required.

4. Conclusions

Tin doping promotes amorphous silicon crystallization only at concentrations exceeding Sn solubility in amorphous silicon (Sn concentration ~1…2 at.%). Prerequisite of Sn induced crystallization of amorphous Si is the available metallic tin clusters. The dominant size of Si crystals formed in the result of tin doping is 2 to 4 nm at the temperature of Si:Sn alloy film formation 200…300 °C. The volume fraction of the crystalline phase depends on the level of doping and may be as high as 80%. Tin impact is efficient enough to transform most of silicon from amorphous to nanocrystalline state within a few minutes of exposition of the alloy film at 200…300 °C during its formation. The likely mechanism of tin influence on $a-Si$ crystallization is eutectic “exchange layer” formed at the interface of metal drop – amorphous semiconductor.

References

1. M.A. Green, K. Emery, Y. Hishikawa, W. Warta, Solar cell efficiency tables (version 37) // *Prog.Photovolt.: Res. Appl.* **19**(1), p. 84-92 (2011); doi: 10.1002/pip.1088.
2. J. Y. Ahn, K.H. Jun, K.S. Lim, M. Konagai, Stable protocrystalline silicon and unstable micro-crystalline silicon at the onset of a microcrystalline regime // *Appl. Phys. Lett.* **82**, p. 1718-1720 (2003); http://dx.doi.org/10.1063/1.1561161
3. A.V. Shah, H. Schade, M. Vanecek, J. Meier, E. Vallat-Sauvain, N. Wyrsch, U. Kroll, C. Droz, J. Bailat, Thin-film silicon solar cell technology // *Prog. Photovolt.: Res. Appl.* **12**, p. 113-142 (2004); doi: 10.1002/pip.533.
4. V.B. Neimash, A. Kraitchinskii, M. Kras’ko, O. Puzenko, C. Claeys, E. Simoen, B. Svensson and A. Kuznetsov, Influence of tin impurities on the generation and annealing of thermal oxygen donors in Czochralski silicon at 450 °C // *J. Electrochem. Soc.* **147**(7), p. 2727-2733, (2000). doi: 10.1149/1.1393596
5. V.B. Neimash, A.M. Kraitchinskii, M.M. Krasko, O.O. Puzenko, O.M. Kabaldin, Influence of tin impurities of the generation and annealing of low-temperature thermal oxygen donors in Czochralski silicon // *Ukr. J. Phys.* **45**(3), p. 342-349 (2000).
6. C. Claeysa, E. Simoena, V.B. Neimash, A. Kraitchinskii, M. Kras’ko, O. Puzenko, A. Blondeel and P. Clauws, Tin doping of silicon for controlling oxygen precipitation and radiation hardness // *J. Electrochem. Soc.* **148**(12), p. G738-G745 (2001); doi:10.1149/1.1417558.
7. E. Simoen, C. Claeys, V. B. Neimash, A. Kraitchinskii, N. Krasko, O. Puzenko, A. Blondeel, and P. Clauws, Deep levels in high-energy proton-irradiated tin-doped n-type Czochralski silicon // *Appl. Phys. Lett.* **76**(20), p. 2838-2840 (2000); http://dx.doi.org/10.1063/1.126490.
8. E. Simoen, C. Claeys, A.M. Kraitchinskii et al. // *Solid State Phenomena*, **82-84**, p. 425-430 (2002).
9. V.V. Voitovych, V.B. Neimash, N.N. Krasko, A.G. Kolosiuk, V.Yu. Povarchuk, R.M. Rudenko, V.A. Makara, R.V. Petrunya, V.O. Juhimchuk, V.V. Strelchuk, The effect of Sn impurity on the optical and structural properties of thin silicon films // *Semiconductors*, **45**(10), p. 1281-1285 (2011); DOI 10.1134/S1063782611100253.
10. V.B. Neimash, V.M. Poroshin, A.M. Kabaldin, V.O. Yukhymchuk, P.E. Shepeliavyi, V.A. Makara, S.Yu. Larkin, Microstructure of thin Si-Sn composite films // *Ukr. J. Phys.* **58**(9), p. 865-871 (2013).
11. E. Bustarret, M.A. Hachicha, and M. Brunel, Experimental determination of the nanocrystalline volume fraction in silicon thin films from Raman spectroscopy // *Appl. Phys. Lett.* **52**, p. 1675-1677 (1988); http://dx.doi.org/10.1063/1.99054.
12. H. Richter, Z.P. Wang, L. Ley, The one phonon Raman spectrum in microcrystalline silicon // *Solid State Communs.* **39**(5), p. 625-629 (1981); http://dx.doi.org/10.1016/0038-1098(81)90337-9.
13. I.H. Campbell, P.M. Fauchet, The effects of microcrystal size and shape on the one phonon Raman spectra of crystalline semiconductors // *Solid State Communs.*, **58**(10), p. 739-741 (1986); http://dx.doi.org/10.1016/0038-1098(86)90513-2.
14. Md.A. Mohiddon, M.G. Krishna, Growth and optical properties of Sn-Si nanocomposite thin films // *J. Mater. Sci.* **47**(19), p. 6972-6978 (2012); DOI: 10.1007/s10853-012-6647-0.
15. M.A. Mohiddon, M.G. Krishna, Chap.17: Metal Induced Crystallization, in: *Crystallization – Science and Technology,* p. 461-480, Ed. Dr. Marcello Andreeta, InTech, 2012; DOI: 10.5772/50064. Available from: http://www.intechopen.com/books/crystallization-science-and-technology/metal-induced-crystallization-of- $a-Si$.
16. R.A. Swalin, *Thermodynamics of Solids.* 2nd ed. Jon Wiley and Sons, New York, 1972.

© 2013, V. Lashkaryov Institute of Semiconductor Physics, National Academy of Sciences of Ukraine